First-time observation of Timelike Compton Scattering

Pierre Chatagnon* and Silvia Niccolai
IJCLab

Stepan Stepanyan
Jlab

(CLAS Collaboration)
(Dated: June 11, 2021)

We present the first observation of the Timelike Compton Scattering (TCS) process, $\gamma p \to \gamma^* p' \to e^+e^-p'$, measured with the CLAS12 detector at Jefferson Lab. The initial photon polarization and the decay lepton angular asymmetries are reported in the range of timelike photon virtualities $2.25 < Q'^2 < 9$ GeV^2 and the squared momentum transferred $0.1 < -t < 0.8$ GeV^2 at the average total center-of-mass energy squared of $\bar{s} = 14.5$ GeV^2. The photon polarization asymmetry, similar to the beam-spin asymmetry in Deeply Virtual Compton Scattering (DVCS), projects out the imaginary part of the Compton Form Factors (CFF) and provides a way to test the universality of Generalized Parton Distributions (GPDs). The angular asymmetry of the decay leptons, on the other hand, accesses the real parts of the CFF that contain the D-term in the parametrization of GPDs.

More than 99% of the mass of the observable universe comes from protons and neutrons. The mass of nucleons comes mainly from the interactions between their fundamental constituents, the quarks and the gluons (also referred to as "partons"), which are described by the Quantum Chromo Dynamics (QCD) Lagrangian. In spite of the recent progress in Lattice QCD, QCD-based calculations cannot yet be performed to explain the properties of nucleons in terms of their constituents. Phenomenological functions are used to connect experimental observables with the dynamics of partons in nucleons. Typical examples of such functions are the form factors (FF) and parton distribution functions (PDF). Generalized Parton Distributions (GPDs) combine and extend the information contained in FF and PDF. They describe the correlations between the longitudinal momentum and transverse spatial position of the partons inside the nucleon, they give access to the contribution of the orbital momentum of the quarks to the nucleon, and they are sensitive to the correlated q-$\bar{q}$ components [1–6].

Compton scattering has long been identified as a golden process among deep exclusive reactions to study GPDs experimentally. The deeply virtual Compton scattering (DVCS), electroproduction of a real photon ($ep \to e'p'\gamma$), has been insofar the preferred tool for accessing GPDs [7–12]. Another Compton process, the timelike Compton scattering (TCS), has been widely discussed theoretically [13–15] but was never measured experimentally. This article reports on the first observation of TCS on the proton. TCS ($\gamma p \to \gamma^* p' \to e^+e^-p'$), is the time-reversal symmetric process to DVCS where the incoming photon is real and the outgoing photon has large timelike virtuality. In TCS, the virtuality of the outgoing photon, $Q'^2 \equiv M^2$, where M is the invariant mass of the lepton pair, sets the hard scale. In the regime $\frac{-t}{Q'^2} << 1$, where t is the squared momentum transfer to the target proton, the factorization theorem will apply (left panel of Fig. 1). The TCS amplitude can then be expressed as a convolution of the hard scattering kernels with GPDs appearing in Compton Form Factors (CFFs). As in the case of DVCS, the Bethe-Heitler process contributes to the same final state (Fig. 1, right). The unique feature of TCS is that with circularly polarized photons it accesses both the real and imaginary parts of CFFs.

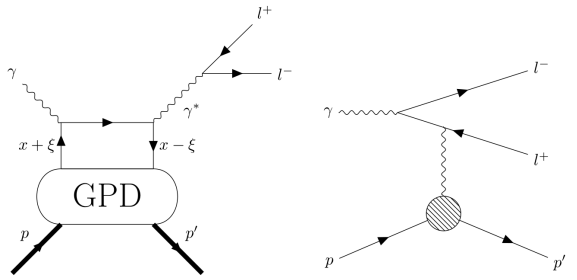

FIG. 1. Left: handbag diagram of the TCS process; right: diagram of the Bethe Heitler (BH) process. Here $x + \xi$ and $x - \xi$ are the longitudinal momentum fractions of the struck quark before and after scattering, respectively, and $t = (p' - p)^2$ is the squared four-momentum transfer between the initial and final protons.

The cross section for lepton pair photoproduction can be expressed as:

$$\sigma(\gamma p \to p' e^+ e^-) = \sigma_{BH} + \sigma_{TCS} + \sigma_{INT}, \qquad (1)$$

where INT stands for the TCS-BH interference term. As it is presented in [13, 14] , the BH contribution dominates the total cross-section over the one of TCS by two orders of magnitude, in our kinematical range. Therefore, the only practical way to access GPDs with the TCS reaction is to measure observables giving access to the TCS-BH interference. At leading order and leading

twist in QCD, $d\sigma_{INT}$ can be expressed as a linear combination of GPD-related quantities:

$$\frac{d^4\sigma_{INT}}{dQ'^2 dt d\Omega} = A\frac{1+\cos^2(\theta)}{\sin(\theta)}[\cos(\phi)\mathrm{Re}\tilde{M}^{--} - \nu\cdot\sin(\phi)\mathrm{Im}\tilde{M}^{--}], \quad (2)$$

where

$$\tilde{M}^{--} = \left[F_1\mathcal{H} - \xi(F_1+F_2)\tilde{\mathcal{H}} - \frac{t}{4m_p^2}F_2\mathcal{E}\right] \quad (3)$$

and A is a kinematic factor given in [13], ϕ and θ are defined in Figure 2, m_p is the proton mass, F_1 and F_2 are the well-known electromagnetic form factors, and $\mathcal{H}$, $\tilde{\mathcal{H}}$, and $\mathcal{E}$ are the Compton Form Factors (CFF) of the H, $\tilde{H}$, and E GPDs, respectively, which are defined in [13]. The unpolarized term is proportional to the real part of the CFF combination $\tilde{M}^{--}$, while the polarized term is proportional to the circular polarization of the incoming photon ν (equal to ±1 for right-handed (resp.left-handed) polarization) multiplied by the imaginary part of $\tilde{M}^{--}$. As the coefficients of $\tilde{\mathcal{H}}$ and $\mathcal{E}$ in Eq. 3 are suppressed, especially in the kinematics covered at Jefferson Lab (JLab), measuring observables linked to the TCS-BH interference cross section mostly provides access to the real part of the $\mathcal{H}$ CFF.

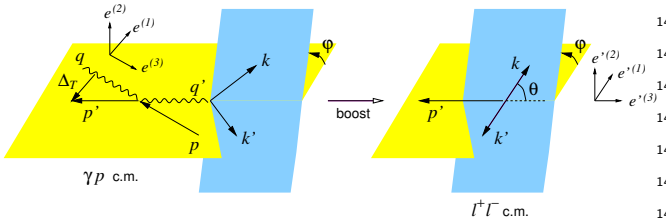

FIG. 2. Kinematic variables and angle definitions for the TCS reaction. The angles ϕ and θ are, respectively, defined as the angle between the leptonic plane (in blue) and the hadronic plane (in yellow), and the angle between the electron and the recoiling proton in the leptons center-of-mass frame. Figure reproduced from [13]

In this work, two TCS observables were measured for the first time: the photon polarization asymmetry and the forward-backward asymmetry. The photon polarization asymmetry, defined as:

$$A_{\odot U} = \frac{\sigma^+ - \sigma^-}{\sigma^+ + \sigma^-}, \quad (4)$$

is proportional to the $\sin(\phi)$ moment of the polarized interference cross section and allows to access the imaginary part of $\mathcal{H}$. Here the subscript +/- stand for the right-handed/left-handed polarization of the real photon.

The forward-backward asymmetry A_{FB}, defined as:

$$A_{FB}(\theta,\phi) = \frac{d\sigma(\theta,\phi) - d\sigma(180^\circ-\theta, 180^\circ+\phi)}{d\sigma(\theta,\phi) + d\sigma(180^\circ-\theta, 180^\circ+\phi)}, \quad (5)$$

projects out the $\cos(\phi)$ moment of the unpolarized cross section, proportional to the real part of the CFF $\mathcal{H}$. This asymmetry has the advantage to remove potential false asymmetry arising from the integration over the finite angular coverage of detectors, compared to the cross-section ratio proposed in [13]. Furthermore it was shown in [16] that the QED radiative corrections are negligible for both of these observables.

The experiment was carried out in Hall B at Jefferson Lab, using a 10.6-GeV electron beam, produced by the CEBAF accelerator, impinging on a 5-cm-long liquid-hydrogen target placed at the center of the solenoid magnet of CLAS12 [17]. Potential quasi-real photoproduction events ($ep \to e^+e^-p'X$) were selected with one reconstructed electron, one positron and one proton. The trajectories of charged particles, bent by the torus and solenoid magnetic fields of CLAS12, were measured by the Drift Chambers (DC) and in the Central Vertex Tracker (CVT), providing the charge and momentum of each track. The electrons and positrons were identified combining the information from the High-threshold Cherenkov counters (HTCC) and the Forward Electromagnetic Calorimeters (ECAL) [18]. A 1-GeV cut on the minimimum lepton momentum is applied to remove the poorly reconstructed tracks in the Forward Detector (FD). The background due to positive pions in the positron sample was minimized by means of a neural-network-based multi-variate analysis of transverse and longitudinal profile of showers in the ECAL. The protons were identified by analyzing the β of positive tracks measured by the CLAS12 time-of-flight systems (FTOF, CTOF) as a function of their momentum. The momenta of the protons were corrected for energy loss in the detector materials using Monte Carlo simulations. Additional data-driven corrections were included, to account, in the case of the leptons, for radiative losses, and, in the case of protons, for detector-dependent momentum shifts not accounted by the simulation.

Once the e^-e^+p events were selected, exclusivity cuts were applied to ensure to be in the quasi-real photoproduction regime. The 4-momenta of the scattered electron and initial real photon are fully defined by the measurement of the 4-momenta of the final state particles. Hence the mass and the transverse momentum fraction of the scattered electron are constrained to be close to zero. The transverse momentum cut ensures that the virtuality of the incoming photon is low ($Q^2 < 0.15$ GeV^2), as it can be written:

$$Q^2 = 2E_bE_X(1-\cos(\theta_X)), \quad (6)$$

where E_b is the energy of the electron beam, E_X is the energy of the undetected scattered electron and θ_X is its scattering angle in the lab frame.

The invariant mass spectrum of the lepton pair after exclusivity cuts is shown in Figure 3. The vector me-

son resonances decaying into an electron-positron pair are clearly visible.

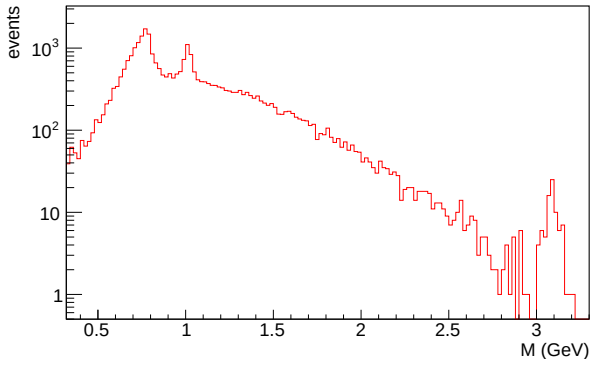

FIG. 3. Invariant mass spectrum of the electron-positron pairs. The peaks correspond to the ρ_0/ω, ϕ and J/ψ mesons. The events corresponding to masses above 1.5 GeV were retained to compute the TCS observables.

The events with invariant mass between 1.5 GeV and 3 GeV were selected to measure the TCS observables. Indeed in this region, the factorization condition $-t/Q'^2 < 1$ for GPD formalism to apply is fulfilled. In Figure 4, the experimentally measured invariant mass distribution is compared with BH Monte-Carlo events. The good agreement between the two distributions rules out the possible contamination of the data by high mass meson resonances decaying into e^+e- pairs (e.g. $\rho(1450)$ and $\rho(1700)$).

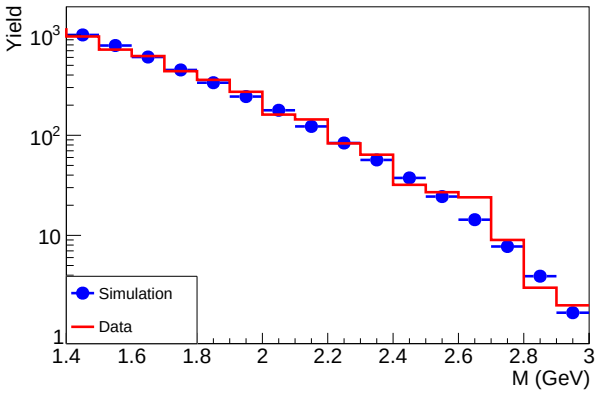

FIG. 4. Data-Simulation comparison of the invariant mass spectrum of the electron-positron pairs in the mass range above 1.4 GeV. The MC histogram is normalised to the total number of events. The bin-by-bin ratio agrees at the 15% level.

The photon polarization asymmetry was computed in four bins of $-t$. Each bin have a equal number of events to yield comparable statistics uncertainties. As this analysis is done on quasi-real photoproduction events, where the real photon is radiated by the initial electron beam, the circular polarization of the photon can be inferred from the initial longitudinal polarization of the electron beam. An electron polarized in the direction (opposite) of the beam emits a right-(left-) handed circularly polarized photon, with a polarization transfer $Pol_{transf.}$ that can be calculated analytically in QED [19]. Taking advantage of this polarization transfer, the asymmetry $A_{\odot U}$ is measured as:

$$A_{\odot U}(-t, E\gamma, M; \phi) = \frac{1}{Pol_{eff}} \frac{N^+ - N^-}{N^+ + N^-}, \qquad (7)$$

where the number of events with reported positive N^+ (resp. negative N^-) electron helicity in each bin is corrected by the acceptance (Acc) and the polarization transfer as:

$$N^{\pm} = \sum \frac{1}{Acc} Pol_{transf.}. \qquad (8)$$

The Pol_{eff} factor accounts for the effective polarization of the CEBAF electron beam. The acceptance and efficiency of CLAS12 (Acc) for the $\gamma p \to e^- e^+ p'$ reaction were estimated using the CLAS12 GEANT-4 based simulations framework [20]. A Monte-Carlo sample of 36 million generated events was used. The acceptance was calculated in 5-dimensional bins corresponding to the five variables describing TCS. In a given bin, the acceptance is defined as the number of events reconstructed in this bin divided by the number of events generated in this bin. Bins with acceptance below 5% are removed and a cut at 50% on the relative error of the acceptance is applied.

The obtained ϕ-distributions of the asymmetry in Equation 7 are shown in Figure 5. The distributions are fitted with a sinusoidal function. In Figure 6, the $-t$ dependence of the amplitude of the sinusoidal modulation is presented.

In-depth systematic checks were performed to validate this measurement. For each identified source of systematic uncertainty, a value of systematic shift is calculated for each bin and added in quadrature after a smoothing procedure. This procedure is necessary to avoid the large fluctuations of the systematic uncertainties from bin-to-bin due to the low statistics of this analysis. Six sources of systematic uncertainties were studied: the uncertainty associated to the binning of the acceptance corrections, the uncertainties associated with the Monte Carlo model used to calculate the acceptance and the related efficiency corrections. The systematic shifts induced by the identification procedure of protons and positrons were also studied. Finally, the impact of the variation of the exclusivity cuts was assessed.

In Figure 6, a clear photon beam polarization asymmetry is observed. This observation is in agreement with the expected contribution of the BH-TCS interference term to the cross section as the expected asymmetry for the

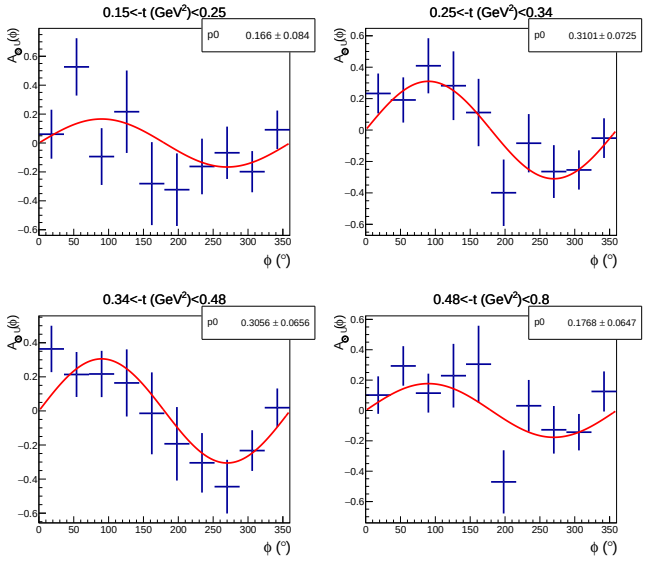

FIG. 5. Photon polarization asymmetry as a function of ϕ for the four t-bins used in this analysis. The fit function is superimposed. The amplitude of the fit p_0 is then plotted as a function of $-t$.

BH contribution only, which was estimated using BH-only Monte-Carlo simulation, is vanishing.

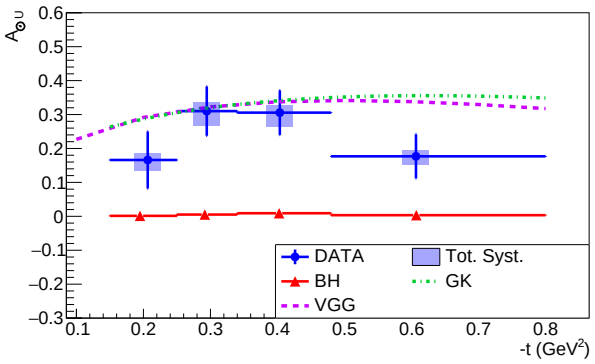

FIG. 6. Photon polarization asymmetry $A_{\odot U}$ as a function of $-t$ and for averaged kinematic point $E_\gamma = 7.29 \pm 1.55$ GeV; $M = 1.8 \pm 0.26$ GeV. The data points are represented in blue with statistical vertical error bars and horizontal error bars representing the bin width. The shaded error bars show the total systematic uncertainty. The red triangles represent the expected value of the asymmetry if only the BH amplitude was contributing to the cross section. Finally, the dashed line is the prediction of the VGG model, and the dashed-dotted line is the prediction of the GK model evaluated at the average kinematic point.

The extracted photon polarization asymmetries was compared to predictions of the VGG model (based on double-distribution parametrization with Regge-like t-dependence) [21–23] and of the GK model (based on the double-distribution paramerization with t-dependence expressed in the forward limit) [24–26], computed within the *PARTONS* framework [27]. Both these calculations are performed at leading order in α_s, albeit QCD corrections have been shown to be quite important [28–30]. The measured values are in agreement with the predictions of GPD based models while BH only calculations show no asymmetry. This observation tend to validate the application of the GPD formalism to describe TCS data and hints to the universality of the GPDs, as the VGG and GK models also describe well the 6-GeV DVCS data from JLab [31].

Using the same data set, the FB asymmetry was measured in four bins of $-t$. The angular coverage of CLAS12 allows to measure this asymmetry only in a limited subset of angles. The FB asymmetry was extracted in the forward direction defined as: $-40° < \phi_0 < 40°$, $50° < \theta_0 < 80°$ with the corresponding backward limits being: $140° < 180° + \phi_0 < 220°$, $100° < 180° - \theta_0 < 130°$. The value of A_{FB} is calculated as:

$$A_{FB} = \frac{N_F - N_B}{N_F + N_B} \tag{9}$$

where $N_{F/B}$ are the number of events in the forward (backward) angular bins, corrected by the acceptance and the bin volume. The bin volume correction accounts for the difference in coverage between the forward and the backward direction that can be the source of false asymmetries. This correction assumes that the cross section of the TCS reaction is relatively constant within the volume of the forward (resp. backward) bin and that it can be estimated only by measuring it in the volume covered by the acceptance of CLAS12. This hypothesis was later verified by extracting the asymmetry with BH-weighted simulated events and the difference between the expected value (null asymmetry) and the extracted value was assigned as a systematic uncertainty.

The extracted FB asymmetry for the whole mass region is shown in Figure 7. In order to explore the hard scale dependence ($Q'^2 \equiv M^2$) of the FB asymmetry, it was extracted separately for the lepton invariant mass region 2 GeV to 3 GeV. The results for the high mass region are shown in Figure 8. The asymmetries in both kinematic regions are not comparable with the vanishing asymmetry predicted if only the BH process was contributing to the total cross-section. This is a confirmation of the TCS diagram contributing to the $\gamma p \to p' e^+ e^-$ cross section.

The experimental results were compared with model predictions. The asymmetries seem to be better described by the VGG model when the D-term (taken from [32]) is included, although error bars are still too large to completely rule out the case without the D-term. The GK model prediction largely underestimate the asymmetry in both mass regions. This could be explained by the absence of D-term in this prediction. The comparison

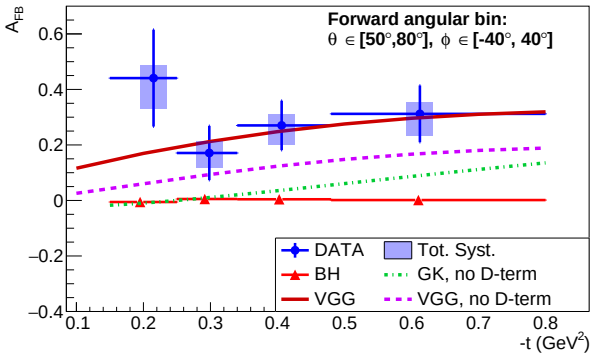

FIG. 7. FB asymmetry as a function of $-t$ at the average kinematics $E_\gamma = 7.23 \pm 1.61$ GeV; $M = 1.81 \pm 0.26$ GeV. The plain line shows the model prediction for the VGG model with D-term (from [32]) evaluated at the average kinematic point.

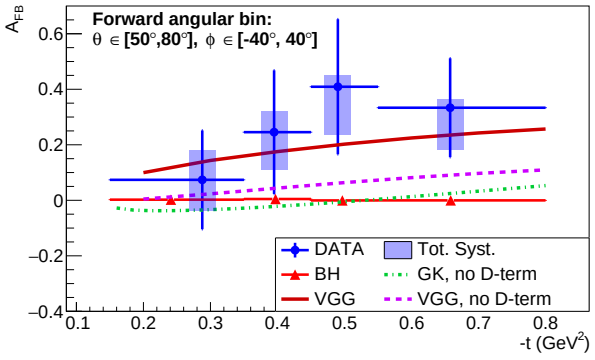

FIG. 8. FB asymmetry as a function of $-t$ at the average kinematics $E_\gamma = 8.13 \pm 1.23$ GeV; $M = 2.25 \pm 0.20$ GeV.

was also done in the high-mass region in Figure 8. In this region, where the factorization condition is stronger, the previous conclusion stands, supporting the interpretation in terms of GPDs and the importance of the D-term in their modelization.

In summary, we reported in this letter the first ever measurement of Timelike Compton scattering. Both the photon circular polarization asymmetry and Forward/Backward asymmetry were extracted. The measured asymmetries are clearly non-zero providing strong evidence for the contribution of the quark-level diagrams parametrized by GPDs to the cross section of this reaction. The comparison of the measured polarization asymmetry with model predictions points toward the interpretation of GPDs as universal functions. Furthermore the reported results on the FB asymmetry open a new promising path toward the extraction of the real part of $\mathcal{H}$, and ultimately to a better understanding of the mechanical properties of the proton via the extraction of the D-term. Future measurements of TCS at JLAB will provide a wealth of data to be included in the ongoing fitting efforts to extract CFFs [33–35]. In particular, TCS measurements will have a strong impact in constraining the real part of CFFs and in the determination of the D-term that relates to the gravitational form factor of the nucleon [36, 37]. A comparison of these results with the future measurements of TCS at the EIC [38] and in ultra peripheral collisions at the LHC [39] could prove useful to better understand the behaviour of the CFFs of TCS at low x [29, 30].

We thank Profs. M. Vanderhaeghen, B. Pire, and P. Sznajder for the fruitful exchanges and discussions on the phenomenological aspects of this work. We acknowledge the great efforts of the staff of the Accelerator and the Physics Divisions at Jefferson Lab in making this experiment possible. This work is supported in part by the U.S. Department of Energy, the National Science Foundation (NSF), the Italian Istituto Nazionale di Fisica Nucleare (INFN), the French Centre National de la Recherche Scientifique (CNRS), the French Commissariat pour l'Energie Atomique, the UK Science and Technology Facilities Council, the National Research Foundation (NRF) of Korea, the Helmholtz-Forschungsakademie Hessen für FAIR (HFHF) and the Ministry of Science and Higher Education of the Russian Federation. The Southeastern Universities Research Association (SURA) operates the Thomas Jefferson National Accelerator Facility for the U.S. Department of Energy under Contract No. DE-AC05-06OR23177.

* chatagnon@ipno.in2p3.fr

[1] D. Müller, D. Robaschik, B. Geyer, F.-M. Dittes, and J. Hořejši, Fortsch. Phys. **42**, 101 (1994).
[2] X. Ji, Phys. Rev. Lett. **78**, 610 (1997).
[3] X. Ji, Phys. Rev. D **55**, 7114 (1997).
[4] A. V. Radyushkin, Phys. Lett. B **449**, 81 (1999).
[5] A. V. Radyushkin, Phys. Rev. D **56**, 5524 (1997).
[6] M. Burkardt, Phys. Rev. D **62**, 071503 (2000).
[7] S. Stepanyan et al. (CLAS), Phys. Rev. Lett. **87**, 182002 (2001).
[8] C. Muñoz Camacho et al. (Jefferson Lab Hall A), Phys. Rev. Lett. **97**, 262002 (2006).
[9] F. X. Girod et al. (CLAS), Phys. Rev. Lett. **100**, 162002 (2008), 0711.4805.
[10] E. Seder et al. (CLAS), Phys. Rev. Lett. **114**, 032001 (2015).
[11] S. Pisano et al. (CLAS), Phys. Rev. D **91**, 052014 (2015).
[12] H. S. Jo et al. (CLAS), Phys. Rev. Lett. **115**, 212003 (2015).
[13] E. Berger, M. Diehl, and B. Pire, Eur. Phys. J. C **23**, 675 (2002).
[14] M. Boër, M. Guidal, and M. Vanderhaeghen, Eur. Phys. J. A **51**, 103 (2015).
[15] P. Nadel-Turonski, T. Horn, Y. Ilieva, F. J. Klein, R. Paremuzyan, and S. Stepanyan, AIP Conf. Proc. **1182**, 843 (2009).
[16] M. Heller, N. Keil, and M. Vanderhaeghen, Phys. Rev.

D **103**, 036009 (2021).
[17] V. D. Burkert et al., Nucl. Instr. Meth. A **959**, 163419 (2020).
[18] V. Ziegler et al., Nucl. Instr. Meth. A **959**, 163472 (2020).
[19] H. Olsen and L. C. Maximon, Phys. Rev. **114**, 887 (1959).
[20] M. Ungaro et al., Nucl. Instr. Meth. A **959**, 163422 (2020).
[21] M. Vanderhaeghen, P. A. M. Guichon, and M. Guidal, Phys. Rev. Lett. **80**, 5064 (1998).
[22] M. Vanderhaeghen, P. A. M. Guichon, and M. Guidal, Phys. Rev. D **60**, 094017 (1999).
[23] M. Guidal, M. V. Polyakov, A. V. Radyushkin, and M. Vanderhaeghen, Phys. Rev. D **72**, 054013 (2005).
[24] S. V. Goloskokov and P. Kroll, Eur. Phys. J. C **42**, 281 (2005).
[25] S. V. Goloskokov and P. Kroll, Eur. Phys. J. C **53**, 367 (2008).
[26] S. V. Goloskokov and P. Kroll, Eur. Phys. J. C **65**, 137 (2009).
[27] B. Berthou et al., Eur. Phys. J. C **78**, 478 (2018).
[28] B. Pire, L. Szymanowski, and J. Wagner, Phys. Rev. D **83**, 034009 (2011).
[29] D. Müller, B. Pire, L. Szymanowski, and J. Wagner, Phys. Rev. D **86**, 031502 (2012).
[30] H. Moutarde, B. Pire, F. Sabatié, L. Szymanowski, and J. Wagner, Phys. Rev. D **87**, 054029 (2013).
[31] R. Dupre, M. Guidal, and M. Vanderhaeghen, Phys. Rev. D **95**, 011501 (2017), 1606.07821.
[32] B. Pasquini, M. Polyakov, and M. Vanderhaeghen, Phys. Lett. B **739**, 133 (2014).
[33] K. Kumericki, S. Liuti, and H. Moutarde, Eur. Phys. J. A **52**, 157 (2016), 1602.02763.
[34] R. Dupré, M. Guidal, S. Niccolai, and M. Vanderhaeghen, Eur. Phys. J. A **53**, 171 (2017), 1704.07330.
[35] H. Moutarde, P. Sznajder, and J. Wagner, The European Physical Journal C **78** (2018).
[36] M. Polyakov, Physics Letters B **555**, 57 (2003).
[37] V. D. Burkert, L. Elouadrhiri, and F. X. Girod, Nature **557**, 396 (2018).
[38] R. A. Khalek, A. Accardi, J. Adam, D. Adamiak, W. Akers, M. Albaladejo, A. Al-bataineh, M. G. Alexeev, F. Ameli, P. Antonioli, et al. (2021), 2103.05419.
[39] B. Pire, L. Szymanowski, and J. Wagner, Phys. Rev. D **79**, 014010 (2009).